ELSEVIER

Contents lists available at ScienceDirect

Ocean Engineering

journal homepage: www.elsevier.com/locate/oceaneng





Dynamic drift-off warning limits for dynamically positioned MODU with Deepwater Artificial Seabed (DAS) system coupling

Xingwei Zhen a,*, Wei Guo b,c, Zhengru Ren d,**, Yi Huang a

- ^a School of Naval Architecture and Ocean Engineering, Dalian University of Technology, Dalian, 116024, China
- ^b China Ship Scientific Research Center, Wuxi, 214082, China
- ^c Taihu Laboratory of Deepsea Technological Science, Wuxi, 214082, China
- d Institute for Ocean Engineering, Shenzhen International Graduate School, Tsinghua University, Shenzhen, 518055, China

ARTICLE INFO

Handling Editor: Prof. A.I. Incecik

Keywords: Artificial seabed Dynamic positioning Drift-off Warning limit MODU

ABSTRACT

A new Deepwater Artificial Seabed (DAS) drilling system, which enables the shallow-water rated drilling equipment to operate in deep and ultra-deep water, has been developed for dynamically positioned Mobile Offshore Drilling Unit (MODU), with a focus on key issues of well access and riser design. Nevertheless, the MODU may drift-off due to the critical failures of the dynamic positioning (DP) system and thus the well integrity will be gravely threatened. This study is committed to establishing the quantitative criteria of drift-off warning limits, which consist of the yellow limit, red limit and physical limit, for dynamically positioned MODU with the coupled DAS drilling system. To achieve this aim, a three-phase methodology is proposed on the basis of a fully coupled model of the MODU-DAS drilling system. Furthermore, a hybrid method integrating the orthogonal experimental design, back propagation neural network, and Garson's algorithm is developed to systematically investigate the importance of the correlative influencing factors on the drift-off warning limits in consideration of both the efficiency and accuracy of the numerical calculations. The validity of the proposed methodology is demonstrated by a case study. The results indicate that the dynamic drift-off warning limits are able to assist in decision-making of safe DP operations on the MODU and the operating depth of the artificial seabed is the most critical factor affecting the envelope of drift-off warning limits. These findings and recommendations could improve the safety of DP drilling operations.

1. Introduction

1.1. Background

At present, deep-water drilling operations call for the surface (dry) or subsea (wet) blow-out preventer (BOP) to control the well safety. The subsea BOP is designed for well control on the sea floor utilizing a 21-inch large-diameter low-pressure drilling riser. As the water depth increases, the weight of the riser and drilling mud also increases, the higher variable deck load, riser storage space, and mud pit volume for the mobile offshore drilling unit (MODU) are required. Subsea BOP typically relies on a fifth or higher generation MODU to support its drilling operations, resulting in relatively high drilling costs. In contrast, surface BOP allows well control on the drilling deck with a 16-inch small-diameter high-pressure drilling riser, which can considerably

reduce the variable deck load, riser storage space, and mud pit volume of MODU. Similarly, the second or third generation MODU can be used to carry out deepwater drilling operations, which can efficiently reduce drilling costs compared to subsea BOP. Nevertheless, surface BOP demands high positioning performance of MODU and slim borehole technology, making it challenging to implement. In conclusion, both the surface and subsea BOP drilling systems encounter their specific challenges due to their own inherent design and operational philosophy (Childers, 2005), as summarized in Table 1.

In response to the challenges of subsea and surface BOP drilling systems, several solutions have been proposed. One such solution is freestanding drilling riser (FSDR) concept, which aims to ensure the storm-safety and minimize the non-drilling time in deep and ultra-deep waters. The FSDR installs a near-surface disconnection package below the mean water level (M.W.L) to allow quick disengagement and

E-mail addresses: zhenxingwei@dlut.edu.cn (X. Zhen), zhengru.ren@sz.tsinghua.edu.cn (Z. Ren).

^{*} Corresponding author.

^{**} Corresponding author.

Table 1Features of subsea BOP vs surface BOP developments in deepwater and ultra-deepwater.

Features	Surface BOP	Subsea BOP
Drilling cost	Inexpensive	Expensive
Drilling efficiency	High-efficient	Inefficient
MODU requirement	Low-cost 2nd, 3rd and 4th generations	Hight-cost 5th generation at least
Drilling riser requirement	High-pressure riser	Low-pressure riser
Well control method	Surface far away wellhead	Seabed close to wellhead
Operating requirement	Special operating requirement	Normal operating requirement
Risk assessment requirement	Extra assessment procedure	Normal assessment procedure

reinstallation of the drilling riser before and after an emergency (Nguyen and Thethi, 2006). Another proposed solution includes the near-surface BOP (Lim et al., 2008) and artificial buoyancy seabed drilling concept (Guo et al., 2006) which are dedicated to improve the drilling capability of drilling rigs. The main principle is to install the BOP on top of a near-surface buoyant tank located below the M.W.L to promote the application of the shallow-water rated drilling technology and equipment in deep and ultra-deep waters. While the FSDR, Near-surface BOP, and artificial buoyancy seabed unit share the common design philosophy of using a near-surface buoyant tank system to disengage the drilling riser. However, the buoyant tank in these concepts is anchored by the lower drilling riser. Once the lower drilling riser is lost, the buoyant tank and the subsurface BOP may ascend towards the MODU, posing a significant threat to the drilling safety.

To address the challenging constraints of the prevailing offshore drilling solutions in deep and ultra-deep water, a cutting-edge Deepwater Artificial Seabed (DAS) drilling concept is proposed by Zhen et al. (2022a), the 2-dimensional and 3-dimensional sketches of the DAS drilling system are illustrated in Fig. 1-(a) and Fig. 1-(b), respectively. The DAS drilling system is designed with a layered-layout scheme consisting of surface, subsurface, and subsea setup, whereby a floating subsurface artificial seabed is anchored by pre-tensioned tendons at a certain depth below the M.W.L BOP stack and wellhead equipment are installed on the artificial seabed by means of a tie-back casing, facilitating the shallow-water rated drilling equipment and technology to be used in deepwater.

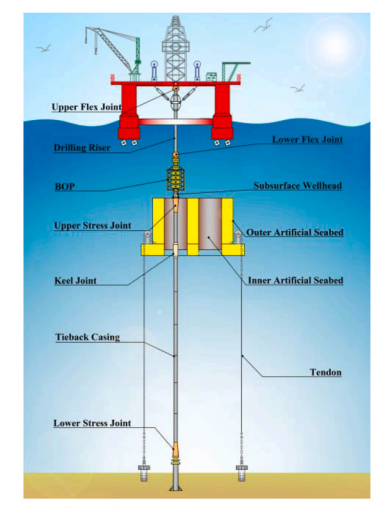
The DAS drilling system mainly consists of four subsystems, including the artificial seabed, the drilling riser, the tieback casing, and the tendons. The main function of the artificial seabed is to support the

tieback casing system and BOP. The artificial seabed comprises the outer artificial seabed and the inner artificial seabed. The outer artificial seabed is designed with a single central column with a skirt. The inner artificial seabed consists of four inner buoyancy cans (IBCs), which are installed inside the outer artificial seabed to support the subsurface wellheads and the BOP. During normal drilling operations, the IBCs are embedded in the outer artificial seabed, the vertical forces and movements between the outer artificial seabed and the IBCs are decoupled. Drilling risers can be benefited from this configuration as they are extremely sensitive to vertical movement. The drilling riser is used to provide circulation channel of drilling mud, protect the drilling pipe, release and retrieve BOP, etc. The drilling riser system consists of multiple units, including upper flex joint, directing acting tensioner, telescopic joint, slick riser, lower flex joint, auxiliary kill and choke lines, etc. The slick riser of the drilling riser system uses the X-80 steel casing. The telescopic joint is used to compensate for the dynamic lifting and compression of the drilling riser system caused by the MODU heave motion. The tieback casing is employed to build the subsurface wellhead, provide circulation channel of drilling mud, protect the drill pipe and guide the drilling units. The tieback casing system includes the slick riser, keel joint, upper stress joint, and lower stress joint, etc. The connecting joints such as the keel joint, upper stress joint, and lower stress joint are designed to mitigate the local stress at their corresponding positions for the tieback casing system. In contrast to the drilling riser system, the slick riser of the tieback casing system uses a high-pressure X-80 steel casing. The tendon is made up of vertically loaded tendons connecting the artificial seabed to the anchor piles. Its primary function is to restrain the horizontal and vertical displacement of artificial seabed. The tendon assemblies consist of three parts, with chains at the bottom and top while tether in the middle.

The critical advantages of the innovative DAS drilling system in deep and ultra-deep waters can be envisaged as follows (Zhen et al., 2022a):

Technical advantages: (1) Reduced technical requirements for the design, manufacture, operation and maintenance of the subsurface wellhead and BOP stack due to their installation on the artificial seabed that is positioned at a shallow-water rated depth. (2) Optimized field layout can be achieved by accommodating numerous subsurface wellheads on the artificial seabed.

Economic advantages: (1) Reduced drilling costs due to the light-weight design and fabrication of the MODU that are achieved due to the enormous loads of the tieback casing are carried by the inner Artificial Seabed. (2) Reduced riser and drilling mud pit storage space as a result of the smaller volume and wet weight of the tieback casing. (3) Improved drilling efficiency due to multiple IBCs are equipped and



(a) 2- dimensional sketch of DAS drilling system



(b) 3- dimensional sketch of DAS drilling system

Fig. 1. Sketches of DAS drilling system (Zhen et al., 2022a).

batch drilling operations can be easily implemented.

Safety advantages: (1) Lowered risks of the subsurface wellhead and the BOP stack from the subsea geological hazards. (2) Improved emergency response performance because the MODU can be quickly disconnected from the artificial seabed in emergency conditions.

1.2. Motivation and objective

The positioning technologies of offshore floating drilling rigs include mooring positioning and dynamic positioning (DP). The former is mainly used in shallow water, while the latter is better for deep and ultra-deep water (Laik, 2018; Ren et al., 2023). The MODU in the DAS drilling system utilizes a DP system for positioning requirements. The operational safety for the DAS drilling system is highly dependent on the DP capability. However, the DP system is susceptible to failures of thrusters, generators, power buses, and the control systems, etc., which can cause uncontrollable drifting of the MODU in case of a blackout. In such situations, the drilling riser must be disconnected timely from the BOP to ensure the safety of drilling equipment. Otherwise, serious consequences such as a breakage of the drilling riser, destruction of wellhead and BOP, collapse of the artificial seabed, and even blowout may occur. According to the International Marine Contractors Association (IMCA) report, there are 1507 incidents caused by DP system during 1990-2014 (IMCA, 2006; IMCA, 2016). In many of these incidents, the drilling equipment such as drilling riser, wellhead, BOP, etc. were damaged to varying degrees, and the oil and gas were eventually released to the sea.

To provide the operator abundant time for the preventive and contingency measures, the drift-off warning limits that can accurately provide guidance for the operation of the emergency disconnect sequence (EDS) should be determined in advance. The graphical representation of drift-off warning limits is presented in Fig. 2. The basic concept in the warning limits is to define the three critical radii around the position of MODU (Chen et al., 2008). The outermost limit, known as the physical limit, is determined by the mechanical limit of the risers and the mooring system. The EDS must be completed and the drilling riser must be disconnected from BOP before the MODU reaches its physical limit. The next smaller red limit is established far enough inside the physical limit radius to provide sufficient time for activating the EDS for safely disconnecting the drilling riser from the BOP. A yellow limit needs to be defined inside the red limit for the preparation of the EDS. In normal operations, the MODU is positioned within the green zone.

The pre-establishment of early drift-off warning limits in the event of loss of station-keeping of the dynamically positioned MODU is central to the safe operation of the DAS drilling system. The main objectives of this paper are twofold: (1) Investigating the dynamic drift-off characteristics of the fully coupled MODU-DAS drilling system so as to establish the dynamic drift-off warning limits of the MODU. (2) Quantifying the

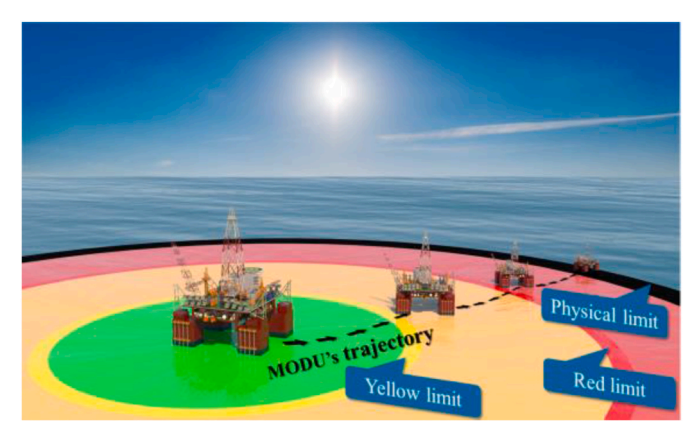


Fig. 2. Graphical representation of drift-off warning limits.

sensitivity of the critical parameters that affect the drift-off warning limits to provide design and operational guidance for the MODU in the DAS drilling system in the event of drift-off scenario.

1.3. Relevant works

DAS drilling system is a new concept of deepwater oil and gas development equipment proposed by Zhen et al. (2022a). The authors performed the conceptual design and analyzed the transient dynamic response study under tendon failure scenarios, which demonstrated the reliability of the DAS drilling system in deepwater. It is worth noting that before the DAS drilling system is proposed. The fundamental research in the design and performance analysis of DAS production system has been conducted for a long time, primarily covering the conceptual design, optimal design, hydrodynamic analysis, and safety control mechanism investigation, etc.

The DAS production system has developed through two generations. The first generation is termed as the Subsurface Tension Leg Platform (STLP), where the artificial seabed is designed in a truss sea-star pontoon configuration (Zhen et al., 2018a). In the latest research (Wu et al., 2019; Zhen et al., 2020, 2022b), it was found that the previous design scheme of the STLP has some technical limitations, such as the strong coupling among the artificial seabed, rigid risers and mooring system. Given this, the structure form of the multi-body configurations of artificial seabed is improved. Compared with the previous design scheme, the IBC is developed to support the subsurface well systems independently and hence decouple the mooring system is decoupled from the subsurface well systems. Subsequently, Wu et al. (2019, 2021) systematically carried out research on the optimal design of the DAS production system and established a multidisciplinary optimization design model considering uncertainties, optimizing the artificial seabed, the flexible jumper, and the riser. A fully coupled numerical model of the floating production unit (FPU)-DAS system was established, and the dynamic response characteristics of the DAS production system under the combined wave-current action was systematically investigated, including mooring system performance analysis, flexible jumper dynamic response analysis, rigid riser dynamic response analysis, interference analysis, strength analysis, buckling analysis and fatigue analysis, etc. (Zhen et al., 2014, 2018a, 2018b; Zhen and Huang, 2017; Zhen et al., 2022). Duan et al. (2022) proposed an analysis method for the coupled dynamic response of moored artificial seabed under the action of internal solitary waves. Numerical simulations and physical model experiments were used to investigate the effects of submergence depth and wave amplitude on the dynamic response of the artificial seabed in an internal solitary wave environment. In addition, the authors also carried out research on the safety control of DAS systems, proposing online risk modelling and decision support principles to add new safety barrier functions to the wellhead system, mooring system, ballast system and external impact protection system of the DAS production system (Zhen et al., 2018c, 2020, 2023). An analysis of the drift warning limits for FPU-DAS coupling was carried out, and the drift-off warning limits for FPU-DAS coupling systems were established, which provides effective guidance for FPUs in power positioning failure scenarios (Han et al., 2021a, 2021b).

In conclusion, the DAS production system has been relatively extensively researched. Nonetheless, the DAS drilling system is required further investigation. One of the key challenges associated with the DAS drilling system is its strongly coupling effects with the MODU, which imposes more demanding drift-off requirements for the MODU when the DP fails. Consequently, it is necessary to specify the safety level of the coupled MODU-DAS drilling system in the case of DP failure based on performing the study of the coupled dynamic drift-off characteristics of the system.

Early research has investigated the drift-off warning issues of MODU in prevailing drilling systems by means of numerical simulations, scaled experiments, risk modelling methods, etc..

There are numerous studies on drift-off warning for MODU, most of which have employed numerical simulations. O'Sullivan et al. (2004) established a fully-coupled drift-off model of vessel/tensioner system/riser/LMRP & BOP/wellhead/conductor/soil. Based on the fully-coupled dynamic analysis, the response results of the offset limiting parameters were obtained to establish the drift-off warning limits of drillship. Bhalla and Cao (2005) developed a procedure to predict the vessel movement trajectory in a drive-off or drift-off event considering environment conditions. Further, the EDS time was used to determine the point of disconnect, red and yellow watch circles. Wang and Donnarumma (2012) studied the drift-off or drive-off scenarios of dynamically positioned drillship in various environmental conditions. The drift-off and drive-off speeds in different environmental conditions were compared to assess the impact of environmental conditions on watch circles. Teixeira et al. (2014) presented a numerical study on drift-off analysis about vessel/riser coupled system, in which the influence of the environmental conditions and initial heading on the offset was analyzed. A revised methodology was proposed by Quigley and Williams (2015) to establish a conservative operability envelope, which combines the steady-state operating limits of the vessel and the transient system response during a drift-off scenario. An extended finite element method for the coupled drift-off and drive-off of a platform was proposed (Liu et al., 2016, 2017, 2019). A coupling numerical model of drilling riser, wellhead and conductor system and a dynamic solver to drift-off & drive-off of the platform were developed respectively. Based on this, the drift-off & drive-off warning limits of the deep-water platform were established. Poirier et al. (2018) introduced the use of dynamic watch circles and dynamic operability envelopes based on real-time monitoring data and actual weather conditions, which enables drilling rig repositioning to optimize the watch circles while maintaining the equipment within the operability criteria.

Some researchers have used scaled experiments to explore the dynamic drift-off characteristics of MODU. Dotta et al. (2018) and Tannuri et al. (2020) presented a validation between the full-scale model test and the numerical simulation for the drift-off of a drilling vessel without risers connected. The model test data have demonstrated the accuracy of the numerical simulation results and confirmed that the simulator is a reliable tool to predict the motion of a drilling vessel after a loss of station-keeping. Xie et al. (2023) conducted the experimental and numerical investigation on self-propulsion performance of polar ship in brash ice channel.

Risk modelling methods are generally utilized to estimate the failure probability. Chen et al. (2008) discussed the failure modes, applicable frequencies, and probabilistic modelling of position loss and recovery based on DP operations of MODU. Influencing factors to the resistance and robustness parameters were identified respectively. Gjerde and Chen (2014) proposed an alternative probabilistic methodology to determine the red watch circle based on probabilistic modelling of position loss scenarios for a DP vessel. Their methodology provided better decision-making support to drillers compared to a red watch circle determined based on the worst scenarios. Chang et al. (2018) explored the emergency disconnection of drilling risers from the perspective of risk assessment. The study indicated the risk influencing factors to the EDS operations and the potential consequences of EDS failure. Nie et al. (2019) proposed a dynamic Bayesian Network and GO model to predict the success probability of RED in the emergency disconnection scenarios of drilling riser over time in different operational stages.

Traditional techniques mainly focus on the physical limit of the conventional drilling system through the dynamic coupled simulations. In particular, the existing studies do not explore the coupling effect of the correlative influencing factors on the drift-off warning limits. It is unable to provide an effective solution to improve the safe operations in a drift-off scenario. This paper aims to propose a three-phase methodology, which is committed to sequentially establishing the quantitative criteria of the physical limit, red limit, and yellow limit based on the scenario. Furthermore, the coupling effect of the correlative influencing

factors on the drift-off warning limits is investigated and the relative importance is determined. The study provides a reference for the Well Specific Operating Guidelines and Restriction Diagrams for the MODU in the DAS drilling system under drift-off scenario. Moreover, the research methodology has reference value to other new offshore structure concepts.

1.4. Structure of the paper

The rest of this paper is organized as follows: Section 2 establishes the theory and associated functions of the dynamic drift-off analysis for the coupled MODU-DAS drilling system. The methodology in terms of constructing dynamic drift-off warning limits and quantifying parameter sensitivity are presented in Section 3. Section 4 details relevant results and discussions. Finally remarks and conclusions are summarized in Section 5.

2. Governing equations

This section will establish the governing equations of the coupled MODU-DAS drilling system. It is assumed that the MODU-DAS drilling system consists of rigid bodies and flexible lines. The governing equations of the two types of structures are established based on their mechanical characteristics. Further, the governing equation of the MODU-DAS drilling system is integrated. The Finite Element Model (FEM) program OrcaFlex (Orcina, 2018) is adopted to establish the numerical calculation model of the MODU-DAS drilling system and solve the governing equation, laying the foundation for the subsequent dynamic drift-off warning investigation of the MODU-DAS drilling system.

2.1. Governing equations of MODU and artificial seabed

The MODU, the outer artificial seabed, and the inner artificial seabed are assumed rigid bodies with six-degree-of-freedom (DOF), and their time domain motion equations can be expressed as follows, respectively

$$\sum_{j=1}^{6} \left[(\boldsymbol{m}_{\text{pla},ij} + \boldsymbol{a}_{\text{pla},ij}(t)) \ddot{\boldsymbol{x}}_{\text{pla},j}(t) + \boldsymbol{B}_{\text{pla},ij} \dot{\boldsymbol{x}}_{\text{pla},j}(t) + \boldsymbol{R}_{\text{pla},ij} \boldsymbol{x}_{\text{pla},j}(t) \right]$$

$$= \boldsymbol{F}_{\text{dri},i} + \boldsymbol{F}_{\text{pla},i} + \boldsymbol{F}_{\text{wav},i} + \boldsymbol{F}_{\text{win},i} + \boldsymbol{F}_{\text{cur},i} \quad i = 1, 2, \dots 6$$
(1)

$$\sum_{j=1}^{6} \left[\left(\boldsymbol{m}_{\text{out},ij} + \boldsymbol{a}_{\text{out},ij}(t) \right) \ddot{\boldsymbol{x}}_{\text{out},j}(t) + \boldsymbol{B}_{\text{out},ij} \dot{\boldsymbol{x}}_{\text{out},j}(t) + \boldsymbol{R}_{\text{out},ij} \boldsymbol{x}_{\text{out},j}(t) \right] \\
= \sum_{j=1}^{6} \left[\left(\boldsymbol{m}_{\text{out},ij} + \boldsymbol{A}_{\text{out},ij} + \boldsymbol{F}_{\text{tra},i} + \boldsymbol{F}_{\text{env},i} \right) + \left(\boldsymbol{A}_{\text{out},ij} \boldsymbol{x}_{\text{out},j}(t) \right) \right]$$
(2)

$$\sum_{j=1}^{6} \left[\left(\boldsymbol{m}_{\text{inn},ij} + \boldsymbol{a}_{\text{inn},ij}(t) \right) \ddot{\boldsymbol{x}}_{\text{inn},j}(t) + \boldsymbol{B}_{\text{inn},ij} \dot{\boldsymbol{x}}_{\text{inn},j}(t) + \boldsymbol{R}_{\text{inn},ij} \boldsymbol{x}_{\text{inn},j}(t) \right]$$

$$= \boldsymbol{F}_{\text{tie},i} + \boldsymbol{F}_{\text{dri},i} + \boldsymbol{F}_{\text{inn},i} + \boldsymbol{F}_{\text{tra},i} + \boldsymbol{F}_{\text{env},i} \quad i = 1, 2, \dots 6$$
(3)

where the subscripts pla, out, and inn refer to the MODU, the outer artificial seabed and the inner artificial seabed, respectively, subscripts i and j represent the indices of the selected DOFs; $[m_{ij}]$ is the mass matrix; $[a_{ij}]$ is the additional quality matrix; $[B_{ij}]$ is the damping matrix; $[R_{ij}]$ is the restoring force coefficient matrix; F_{tet} , F_{tie} , and F_{dri} are the response forces of the tendon, tieback casing, and drilling riser system, respectively; F_{tra} is the interaction force between the outer platform and the inner buoy of the artificial seabed; F_{out} and F_{inn} are the buoyancy of the outer platform and the inner buoy of the artificial seabed; F_{env} is the hydrodynamic loads; F_{wav} , F_{win} , and F_{cur} represent the loads of wave, wind, and current, respectively.

2.2. Governing equations of riser and tendon

The risers (including the drilling riser and the tieback casing) and the tendon are flexible structures, their governing equations can be expressed as

$$EI\frac{\partial^{4} \delta}{\partial z^{4}} - \frac{\partial}{\partial z} \left(T_{e} \frac{\partial \delta}{\partial z} \right) + C \frac{\partial \delta}{\partial t} + M \frac{\partial^{2} \delta}{\partial t^{2}} = F_{\text{env}}$$
(4)

$$C\frac{\partial \delta}{\partial t} + M\frac{\partial^2 \delta}{\partial t^2} - \frac{\partial}{\partial z} \left(T_e \frac{\partial \delta}{\partial z} \right) = F_{env}$$
 (5)

where EI is the bending stiffness; δ is the displacement; $T_{\rm e}$ is the effective tension; C is the structural viscous damping factor; and M is the mass of per unit length.

The effective tension is given by

$$T_{\rm e} = T + A_{\rm o}P_{\rm o} - A_{\rm i}P_{\rm i} \tag{6}$$

$$T = E(A_{\rm o} - A_{\rm i})\sigma \tag{7}$$

where T is the actual tension of the risers or tendons; $A_{\rm o}$ and $A_{\rm i}$ represent the external and internal cross-sectional areas of the risers, respectively; $P_{\rm o}$ and $P_{\rm i}$ are the external and internal pressures on the risers, respectively, and σ is the average axial strain.

2.3. Equations of environmental loads

Hydrodynamic loads on the artificial seabed system, risers and mooring system are calculated by means of an extended form of the Morison equation as follows (Morison et al., 1950)

$$F_{\text{env}} = \left(\Delta a_{\text{f}} + C_{\text{a}} \Delta a_{\text{r}}\right) + \frac{1}{2} \rho_{\text{wat}} C_{\text{d}} A v_{\text{r}} |v_{\text{r}}|$$
(8)

where Δ is the mass of fluid displaced by the body; a_f is the fluid acceleration relative to earth; C_a is the added mass coefficient for structures; a_r is the fluid acceleration relative to structures; $\rho_{\rm wat}$ is the density of water; $\nu_{\rm r}$ is the fluid velocity relative to structures; $C_{\rm d}$ is the drag coefficient for the structures, and A is the drag area.

The drift-off motion of the MODU is influenced by loads of wind, current, wave, subsea systems force and thruster force. The calculation of the wind and current loads on the MODU is performed according to the recommendations of the Oil Companies International Marine Forum (OCIMF, 1994), given by

$$F_{\text{win/cur}} = \begin{bmatrix} f_x \\ f_y \\ f_z \end{bmatrix} = \begin{bmatrix} \frac{1}{2} C_{\text{surge}} \rho_{\text{win/cur}} |v|^2 A_{\text{surge}} \\ \frac{1}{2} C_{\text{sway}} \rho_{\text{win/cur}} |\mathbf{v}|^2 A_{\text{sway}} \\ \frac{1}{2} C_{\text{heave}} \rho_{\text{win/cur}} |v|^2 A_{\text{heave}} \end{bmatrix}$$
(9)

$$M_{\text{win/cur}} = \begin{bmatrix} m_x \\ m_y \\ m_z \end{bmatrix} = \begin{bmatrix} \frac{1}{2} C_{\text{roll}} \rho_{\text{win/cur}} |\nu|^2 A_{\text{roll}} \\ \frac{1}{2} C_{\text{pitch}} \rho_{\text{win/cur}} |\nu|^2 A_{\text{pitch}} \\ \frac{1}{2} C_{\text{yaw}} \rho_{\text{win/cur}} |\nu|^2 A_{\text{yaw}} \end{bmatrix}$$

$$(10)$$

where f_x , f_y , and f_z are the drag forces in the x-, y-, and z-directions, respectively; m_x , m_y , and m_z are the moment in the x-, y-, and z-directions, respectively; C_{Surge} , C_{Sway} , C_{heave} , C_{roll} , C_{pitch} , and C_{yaw} are the surge, sway, heave, roll, pitch, and yaw coefficients for the current or wind direction relative to the vessel heading, respectively; $\rho_{win/cur}$ is the density of current or wind, and ν is the relative velocity of the current or wind passing the vessel.

The wave loads on the MODU can be calculated by

$$F_{\text{wav}} = \begin{bmatrix} F_{\text{wav,1st}} \\ F_{\text{wav,2nd}} \end{bmatrix} = \begin{bmatrix} \int S(w) \text{RAO}(w, \beta_{\text{wav}}) dw \\ \int S(w) \text{QTF}(w, \beta_{\text{wav}}) dw \end{bmatrix}$$
(11)

where $F_{\text{wav},1\text{st}}$ and $F_{\text{wav},2\text{nd}}$ are the first- and second-order wave loads, respectively; S(w) is the wave spectrum for a given sea state; RAO and QTF are the response amplitude operator and quadratic transfer function, respectively; ω is the angular frequency of wave, and β_{wav} is the incident wave direction.

The thruster forces on the MODU are assigned to be zero in this study to simulate a drift-off scenario since all thrusters are in a total-loss-ofeffectiveness failure.

2.4. Governing equation of MODU-DAS coupled system and solving method

The governing equation of the coupled MODU-DAS drilling system can be expressed as follows

$$\mathbf{M}\ddot{\mathbf{x}}(t) + \mathbf{B}\dot{\mathbf{x}}(t) + \mathbf{K}\mathbf{x}(t) = \mathbf{F}(t)$$
(12)

where M is the mass matrix; B is the damping matrix; K is the stiffness matrix; x(t), \dot{x} (t) and \ddot{x} (t) are the position, velocity and acceleration vectors, respectively; F(t) is the external load; and t is the simulation time

In this paper, the OrcaFlex (Orcina, 2018), which employs generalized- α method in combination with the Newton-Raphson iterative method to solve the fully coupled time-domain motion Eq. (12), is used to carry out the fully coupled drift-off analysis of the MODU-DAS drilling system. The numerical simulation model of the MODU-DAS drilling system is shown in Fig. 3.

Assuming that Δt is the iteration time step, x_t and $\dot{x}_{t+\Delta t}$ can be expressed as follows, respectively

$$\mathbf{x}_{t+\Delta t} = \mathbf{x}_t + \Delta t \dot{\mathbf{x}}_t + \Delta t^2 \left[\left(\frac{1}{2} - \beta \right) \ddot{\mathbf{x}}_t + \beta \ddot{\mathbf{x}}_{t+\Delta t} \right]$$
 (13)

$$\dot{\mathbf{x}}_{t+\Delta t} = \dot{\mathbf{x}}_t + \Delta t (1 - \zeta) \ddot{\mathbf{x}}_t + \Delta t \zeta \ddot{\mathbf{x}}_{t+\Delta t} \tag{14}$$

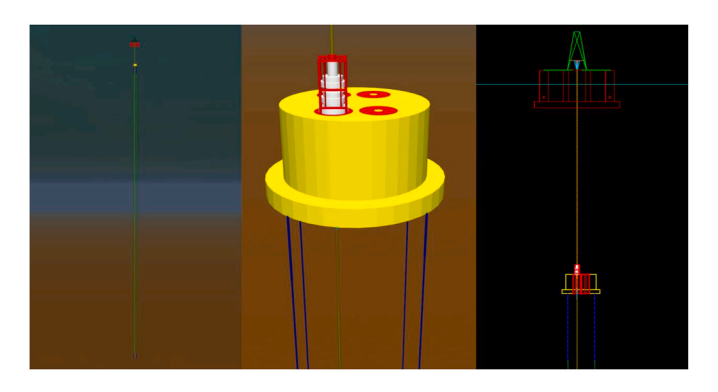
According to the generalized- α method, the time coupled dynamic equilibrium iterative equation of the MODU-DAS drilling system can be expressed as

$$M\left[(1-\alpha_{n})\dot{\mathbf{x}}_{t+\Delta t} + \alpha_{m}\ddot{\mathbf{x}}_{t}\right] + C\left[(1-\alpha_{f})\dot{\mathbf{x}}_{t+\Delta t} + \alpha_{f}\dot{\mathbf{x}}_{t}\right] + K\left[(1-\alpha_{f})\mathbf{x}_{t+\Delta t} + \alpha_{f}\mathbf{x}_{t}\right] = F\left[(1-\alpha_{f})(t+\Delta t) + \alpha_{f}t\right]$$
(15)

$$\alpha_{m} = \frac{2\rho - 1}{\rho + 1}, \alpha_{f} = \frac{\rho}{\rho + 1}$$

$$\beta = \frac{1}{4} (1 + \alpha_{f} - \alpha_{m})^{2}, \zeta = \frac{1}{2} + \alpha_{f} - \alpha_{m}$$
(16)

where $\rho \in [0, 1]$ represents the spectral radius, which is a parameter to control the energy dissipation of the algorithm. The energy dissipation of the algorithm decreases with the increasing ρ . In this paper, ρ takes



 $\begin{tabular}{ll} Fig. 3. Fully coupled numerical simulation model of the MODU-DAS drilling system. \end{tabular}$

the value of 0.4.

According to the generalized- α method, the $x_{t+\Delta t}$, $\dot{x}_{t+\Delta t}$, and $\ddot{x}_{t+\Delta t}$ at the $t+\Delta t$ moment are obtained by performing the following calculation steps:

Step 1 Form the effective stiffness matrix.

$$\widehat{\mathbf{K}} = e_k \mathbf{K} + e_0 \mathbf{M} + e_1 \mathbf{C} \tag{17}$$

Step 2 Compute the effective force at $t+\Delta t$.

$$\widehat{F}(t + \Delta t) = F\left[\left(1 - \alpha_f\right)(t + \Delta t) + \alpha_f t\right] - \alpha_f K x_t + M \left(e_0 x_t + e_2 \dot{x}_t + e_3 \ddot{x}_t\right) + C \left(e_1 x_t + e_4 \dot{x}_t + e_5 \ddot{x}_t\right)$$
(18)

Step 3 Solve the displacement at $t+\Delta t$.

$$\mathbf{x}_{t+\Delta t}^{n} = \widehat{\mathbf{K}}^{-1} \widehat{\mathbf{F}}(t + \Delta t) \tag{19}$$

Step 4 Compute the acceleration and velocity at $t+\Delta t$.

$$\dot{\mathbf{x}}_{t+\Delta t}^{n} = \dot{\mathbf{x}}_{t} + e_{6}\ddot{\mathbf{x}}_{t} + e_{7}\ddot{\mathbf{x}}_{t+\Delta t}^{n} \tag{20}$$

$$\ddot{\mathbf{x}}_{t+\Delta t}^{n} = e_0(\mathbf{x}_{t+\Delta t}^{n} - \mathbf{x}_t) - e_2 \dot{\mathbf{x}}_t - e_3 \ddot{\mathbf{x}}_t$$
 (21)

Step 5 Repeated iterative calculation, the iterative calculation of $t+\Delta t$ is completed until the following conditions are met.

$$\|\boldsymbol{x}_{t+\Delta t}^{n+1} - \boldsymbol{x}_{t+\Delta t}^{n}\| < \mu \tag{22}$$

where, n represents the number of iterations, and μ is a constant that

controls the iteration accuracy.

$$\begin{cases}
e_k = 1 - \alpha_f & e_0 = \frac{1 - \alpha_m}{\beta \Delta t^2} & e_1 = \frac{e_k \zeta}{\beta \Delta t} \\
e_2 = \Delta t e_0 & e_3 = \frac{e_2 \Delta t}{2} - 1 & e_4 = e_k \frac{\zeta}{\beta} - 1 \\
e_5 = e_k \Delta t \left(\frac{\zeta}{2\beta} - 1\right) & e_6 = \Delta t (1 - \zeta) & e_7 = \zeta \Delta t
\end{cases}$$
(23)

After the iterative calculation of the $t+\Delta t$ is completed, the displacement, velocity and acceleration of the structure at next moment time can be calculated by adding the time step Δt and repeating the above steps until the iterative calculation is completed.

3. Methodology

The methodology is developed as illustrated in Fig. 4. It consists of establishing the dynamic drift-off warning limits and quantitatively investigating the parameter sensitivity of the dynamic drift-off warning limits

To establish the dynamic drift-off warning limits, the critical parameters in determining the physical limit of the MODU and their failure criteria are established firstly. Further, the dynamic drift-off analysis of the fully coupled MODU-DAS drilling system is conducted by numerical simulations. The physical limit is determined by the failure criteria of the critical parameters. Finally, the red and yellow limits can be established according to the physical limit and the operating principles of the EDS.

An approach integrating the orthogonal experimental design (OED), back propagation neural network (BPNN), and Garson's algorithm (GA) is proposed to further explore the sensitivity of parameters affecting the drift-off warning limits of the MODU. The OED scheme is used to obtain typical cases of influencing parameters regarding to drift-off warning limits. The numerical simulations for coupled MODU-DAS drilling system are implemented to explore each case to obtain the drift-off warning limits. The BPNN is constructed and trained based on parameter assemblies of the OED and the drift-off warning limits of numerical simulations to obtain the weight coefficients of neural layers. The GA is employed to calculate the relative importance of each influencing

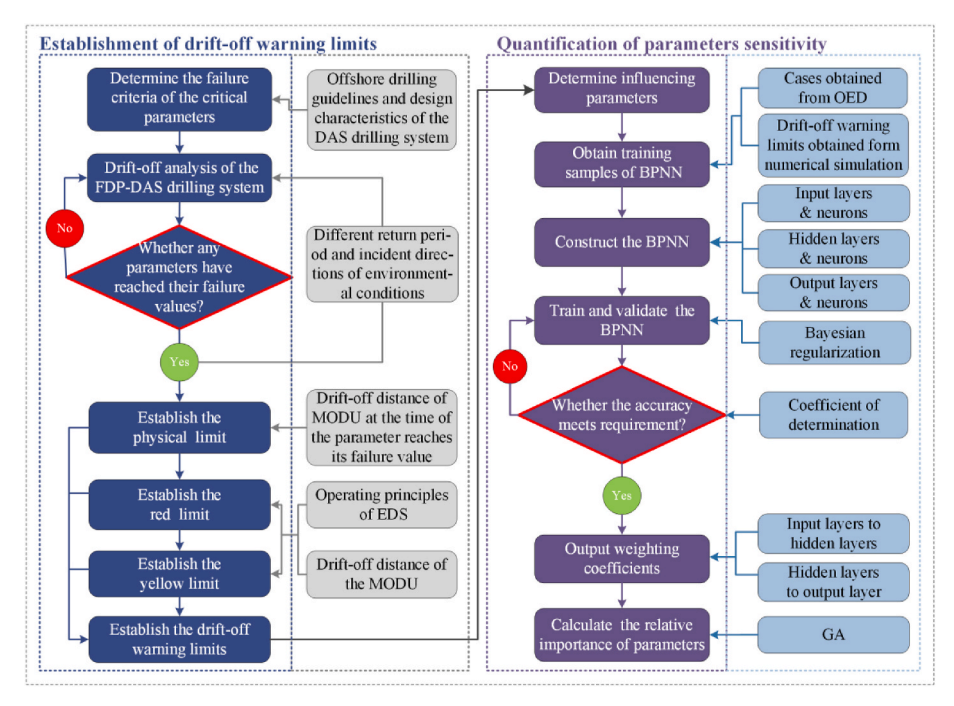


Fig. 4. Flow chart on establishing dynamic drift-off warning limits and quantifying parameters sensitivity.

parameter using the weight coefficient.

3.1. Method for establishing dynamic drift-off warning limits

A three-phase method for establishing dynamic drift-off warning limits of MODU is proposed, as summarized in the following steps.

- (1) Critical parameters in determining the drift-off physical limit of the MODU and their mechanical failure criteria are established based on the characteristics of the DAS drilling system and existing offshore drilling guidelines. These critical parameters are mainly sourced from risers (including drilling riser and tieback casing) guideline API RP 2RD (API, 1998) and tendon systems API RP 2SK (API, 2015), as illustrated in Table 2.
- (2) The drift-off dynamic response characteristics of critical parameters are investigated to determine the physical limit of the MODU according to the parametric mechanical failure criteria. Specifically, a fully coupled numerical simulation model of the MODU-DAS drilling system is established, and dynamic drift-off analysis of the MODU-DAS drilling system is performed using the FEM program to investigate the dynamic response of the critical parameters. The primary objective is to identify the critical parameter, which reaches the mechanical failure criterion firstly during the drift-off process of the MODU, and to obtain the physical limit.
- (3) The red and yellow limits can be established based on the physical limit and the operating principles of the EDS. According to (Liu et al., 2019), it takes 40 s from EDS preparation to EDS activation, and 15 s from EDS activation to EDS completion. The red limit is calculated by subtracting the drift-off distance of the MODU during the period between the activation of the EDS and the completion of the EDS from the physical limit. Then, the yellow limit is calculated by subtracting the drift-off distance during the period from the preparation for EDS to the activation of the EDS from the red limit. Finally, the drift-off warning limits are comprised of a physical limit, a red limit and a yellow limit.

3.2. Method of parameter sensitivity analysis

The objective of conducting parameter sensitivity analysis is to quantify the relative importance of various parameters affecting the drift-off warning limits of the MODU in the DAS drilling system. It is essential for providing guidance on the reliability design of the DAS drilling system in relation to the safe control of the MODU in the event of the drift-off scenarios. The parameters affecting the drift-off warning limits of the MODU in the DAS drilling system can be categorized into design parameters (installation depth of the artificial seabed, the mass of the MODU and rotation stiffness of flex joints, etc.) and environmental parameters (wave height, current and wind velocity, etc.). For instance, in the case of DP failure, the MODU may suffer uncontrollable drift primarily driven by wave, current, and wind loads. Wave height, current speed, and wind speed are three important parameters to characterize

Table 2 Failure criteria of critical parameters.

Parameters	Symbol	Failure value	Unit			
Declination of the upper flex joint	θ_u	9	deg			
Declination of the lower flex joint	θ_l	9	deg			
Physical stroke of the telescopic joint	1	16.76	m			
σ of the drilling riser	$\sigma_{ m d}$	552	MPa			
σ of the tieback casing	σ_{t}	552	MPa			
σ of the keel joint	$\sigma_{ m k}$	552	MPa			
σ of the upper stress joint	$\sigma_{\rm n}$	551	MPa			
σ of the lower stress joint	σ_l	552	MPa			
Safety factor of tendon	λ	1.25	_			
σ represents the Maximum von Mises stress.						

wave, current, and wind loads, respectively. An increase in these three parameters will accelerate the drift-off speed of the MODU, leading to a shorter drift-off time for the MODU reaching the physical limit. Hence, in severe sea conditions, the operator is required to start preparing for the initiation of EDS of the drilling riser as early as possible. Conversely, the initiation of EDS can be delayed. Consequently, exploring the sensitivity of these three parameters can provide effective guidance to the operator during actual drilling operations. However, it is time-consuming to quantitatively investigate parameters sensitivity only using numerical simulation method due to the large number of statistical samples generated for varying environmental parameters and design parameters.

The data-driven method based on artificial neural network (ANN), is widely used for iterative training and learning of data through adaptive learning mechanisms. This approach has been implemented in parameter sensitivity studies in the field of naval architecture and ocean engineering, as demonstrated by several researchers (Quéau et al., 2015; Cheng et al., 2019; Kim et al., 2020; Wang et al., 2021). Nevertheless, ANN cannot be directly used for parameter sensitivity analysis. For this purpose, additional methods should to be utilized. One of the most classical methods for ANN-based parameter sensitivity analysis is the GA, which calculates the sensitivity of parameters based on the connection weight coefficients between neural network layers (Garson, 1991). Normally, ANNs can be categorized into various types based on different network topologies, such as radial basis network, recurrent neural network, convolutional neural network, and BPNN, etc. The BPNN is one of the most utilized ANNs and can predict complex nonlinear systems with single hidden layer generally (Wang et al., 2015). Consequently, the BPNN is utilized in this study for parameter sensitivity analysis.

In this work, an approach of OED-BPNN-GA is proposed to explore the sensitivity of parameters affecting the drift-off warning limits of the MODU. Specifically, the OED is used to obtain typical cases with different combinations of parameters as the input samples of the BPNN. Based on this, the FEM program is used to explore the response results of each representative case of impact parameters to obtain the drift-off warning limits of the MODU as the output samples of the BPNN. Further, the BPNN is trained with the data obtained above and then the weight coefficients of each layer are outputted after the training is completed. Finally, the GA is used to calculate the relative importance of each impact parameter for the drift-off warning limits of the MODU using the weight coefficients.

3.2.1. Orthogonal experimental design

To obtain statistical samples for training the BPNN, numerical simulations of the various combinations of parameters affecting the drift-off physical limit of the MODU are required. Nevertheless, it is computationally prohibitive for performing numerical simulations with all possible combinations of parameters. For example, more than 6500 cases need to be studied if a comprehensive case consists of 9 parameters with 4 different values for each parameter, which will be time-consuming even if computer simulation tools are adopted. To address this issue, the OED is used in this study as it is an effective method to reasonably arrange multi-parameter with multi-level (i.e., multiple different values) experiments. The OED can't only significantly reduce the workload but also ensure the accuracy of the experiments by selecting some representative tests from the comprehensive experiments according to the orthogonality (Wu, 2013).

Constructing an orthogonal table is the key to the OED, which follows the below principles: (1) The number of occurrences of different values in each column of the orthogonal table is equal; (2) If two values in the same row are considered as ordered pairs, the number of occurrences of each pair is equal in any two columns of the orthogonal table. When the number of levels of each parameter is the same i.e. $l_1 = l_2 = l_3 = \ldots = l_q$, the orthogonal table can be abbreviated as $T_p(L^q)$. Where T is the symbol of the orthogonal table, p is the number of cases, L is the

number of parameter levels, and q is the number of parameters.

The critical parameters that affect the drift-off warning limits of the MODU in the DAS drilling system are divided into two categories, i.e., design parameters and environmental parameters, as tabulated in Table 3. In this paper, a $T_{32}(4^9)$ orthogonal table is constructed based on Table 3 to generate 32 numerical simulation cases as the inputs of the BPNN, where each case consists of the above 9 parameters taking different values based on the principle of OED. Then, each case is simulated by the OrcaFlex to obtain the drift-off warning limits as the outputs of the BPNN.

3.2.2. BPNN theory

BPNN is a multilayer mapping network that minimizes errors backward while transmitting information forward. It consists of a series of layers, including an input layer (first layer), multi-hidden layers (intermediate layers), and an output layer (last layer), each of which includes at least one neuron. In general, one hidden layer with adequate neurons is enough to approximate any continuous functions (de Pina et al., 2013). In this study, a single hidden layer BPNN consists of an input layer, a hidden layer, and an output layer is constructed, as illustrated in Fig. 5.

The input layer has 9 neurons representing the 9 parameters as tabulated in Table 3, while one neuron in the output layer represents the drift-off warning limits, i.e., the physical limit, red limit or yellow limit obtained from the numerical simulations. The determination of the number for neurons in the BPNN hidden layer is a very complex problem. It usually needs to be estimated based on the experience of the designer and multiple experiments. In this paper, a reasonable range of neuron values for the hidden layer is determined based on the empirical Eq. (24) firstly (Shen et al., 2008), and then the best training efficiency and accuracy of BPNN is finally obtained by trial-and-error method when the hidden layer contains 10 neurons.

$$n_{\rm i} = \sqrt{n_{\rm h} + n_{\rm o}} + c \tag{24}$$

where n_i , n_h , and n_o are the number of neurons in the input, hidden, and output layers respectively; and c is a constant between [1,10].

The accuracy of the BPNN is evaluated by the R^2 called the coefficient of determination of the test set, which is defined as Eq. (25). The closer the R^2 value is to 1, the higher accuracy of the BPNN.

$$R^{2} = 1 - \frac{\sum_{i_{p}=1}^{n_{p}} \left(y_{i_{p}} - \overline{y}_{i_{p}} \right)^{2}}{\sum_{i_{p}=1}^{n_{p}} \left(y_{i_{p}} - \widehat{y}_{i_{p}} \right)^{2}}$$
 (25)

where n_p is the amount of sample points; y_{i_p} is the actual value of the response; \overline{y}_{i_p} is the mean value of the exact responses; and \hat{y}_{i_p} is the predicted value.

In addition, in order to accelerate the convergence training speed and improve the accuracy of the BPNN, the input sample data need to be normalized according to Eq. (26)

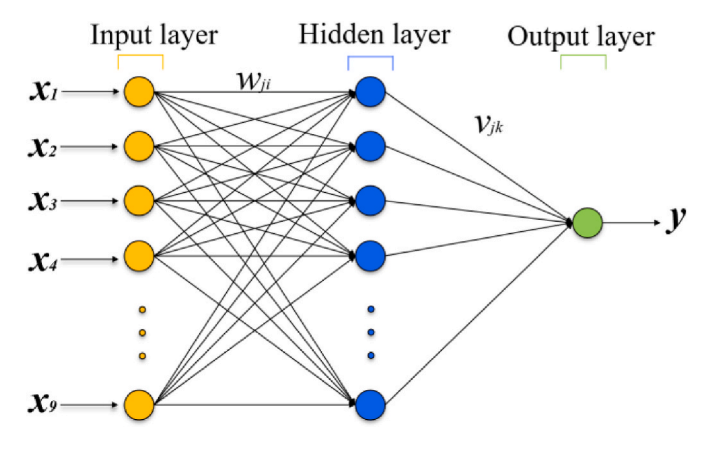


Fig. 5. Topology of the BPNN.

$$\widehat{x}^{(n_0)} = \frac{x^{(n_0)} - \mu}{\sigma} \tag{26}$$

where $x^{(n_0)}$ is the original sample value, σ is the standard deviation value of the samples, μ is mean value of samples, and $\hat{x}^{(n_0)}$ is the standardized value.

3.2.3. Garson's algorithm

The GA is an efficient method for analyzing the structure of ANN. The basic principle of the GA is to calculate the sensitivity of the output parameters to the input parameters using the connection weights between the layers of the ANN. Specifically, the sensitivity of the u-th input parameter to the v-th output can be defined as

$$S_{uw} = \frac{\sum_{v=1}^{L} \left(\left| \omega_{uv} v_{vw} \right| / \sum_{r=1}^{N} \left| \omega_{rv} \right| \right)}{\sum_{r=1}^{N} \sum_{v=1}^{L} \left(\left| \omega_{uv} v_{vw} \right| / \sum_{r=1}^{N} \left| \omega_{rv} \right| \right)}$$
(27)

where S_{uw} represents the relative importance of the u-th input variable to the w-th output variableiable; N and L are the numbers of neurons in the input and hidden layer, ω_{uv} is the connection weight between the input neuron u-th and the hidden neuron v-th, v_{vw} is the connection weight between the hidden neuron v-th and the output neuron w-th.

4. Results and discussions

This section systematically investigates the drift-off dynamic characteristics of the coupling MODU-DAS drilling system under the actual environmental conditions of the 3000-m-deep water in the South China Sea. The detailed information of environmental condition employed in this study is shown in Table 4. It is assumed that the wind, wave, and current propagate in the same direction. The total dynamic analysis time is 150 s, and the time step is set as 0.1 s. Structure parameters of the DAS

Table 3Critical parameters and levels of OED for drift-off warning limits of the MODU in the DAS drilling system.

Type of parameters	Name of parameters	Symbol	Unit	Levels			
				1	2	3	4
Environmental parameters	Wind speed	$V_{ m w}$	m/s	5	10	15	20
•	Current speed	$V_{ m c}$	m/s	0.5	1.0	1.5	2.0
	Significant wave height	$H_{\rm s}$	m	2	4	6	8
	Incident direction	θ	deg	0	30	60	90
Design parameters	Mass of MODU	M	te	8×10^4	10×10^4	12×10^4	14×10^4
	Submerged depth of artificial seabed	D	m	200	250	300	350
	Top Tension Factor	TTF	_	1.2	1.4	1.6	1.8
	Rotational stiffness of upper flex joint	K_{u}	kN·m/deg	150	200	250	300
	Rotational stiffness of lower flex joint	K_1	kN·m/deg	150	200	250	300

Table 4 Environmental conditions.

Return period	Significant wave height (m)	Peak period (s)	Wind velocity (m/s)	Surface current velocity/(m/s)
1-year	6.2	7.5	16.4	1.16
10-year	7.5	7.9	18.6	1.51
50-year	8.5	8.1	20	1.74
100-year	8.9	8.2	20.6	1.85

drilling system are tabulated in Table 5.

4.1. Dynamic drift-off movement investigations of MODU

To investigate the trajectory and motion characteristics of the MODU in the drift-off process, the dynamic drift-off six- DOF motions characteristics of the MODU are analyzed. Fig. 6 presents the drift-off trajectory of the MODU under six-DOF motions in different return periods of environmental conditions, with the incident direction of environmental conditions aligned with the bow. It can be seen from Fig. 6 that the environmental conditions pose a significant impact on the MODU's driftoff trajectory, with harsher environmental conditions resulting in a greater movement amplitude of the MODU. For example, the drift-off displacement of the MODU along the x-axis increases from 113.1 m to 186.9 m with increasing rate of 65.3% at 150s, when the environmental condition's return period increases from 1 year to 100 years. The driftoff displacement of the MODU along the x-axis increases significantly with the drift-off time, while the displacement of the y-axis remains almost unchanged due to the incident direction of environmental conditions being along the x-axis. The dynamic motion amplitude of the MODU along the z-axis presents a periodic variation due to the periodicity of the wave force. Once the drift-off time exceeds 100 s, the motion amplitude of MODU along the z-axis increases significantly, which is owed to the fact that the telescopic supplement system gradually reaches the limiting value, which leads to the decay of the compensation effect on the MODU's motion along z-axis, further resulting in an increasing amplitude of the MODU's vertical motion. It can be seen that there is only a slight amplitude of rotational movements during the drift-off process of the MODU and the maximum value does not exceed 1.5°, which can prove that there is no risk of capsizing for the MODU during the drift-off process. The above analysis shows that the MODU has a significant drift-off motion along the incident direction of environmental conditions, while the motion in the remaining five-DOF is relatively small. It should be noted that when the drift time exceeds 100 s, the vertical motion of the MODU should be monitored to prevent excessive vertical motion amplitude, which may cause excessive stretching or compression of the riser system.

4.2. Dynamic drift-off movement investigations of artificial seabed

In order to investigate the motion characteristics of the artificial seabed in the drift-off process of the MODU and evaluate the stability of the artificial seabed, the six-DOF motions behaviors of the artificial seabed are further analyzed. Fig. 7 presents comparison results of the dynamic behaviors of the 6-DOF movements for the artificial seabed under different return periods of environmental conditions. It can be observed that the amplitude of the 6-DOF motions of the artificial seabed increases with the increase of environmental conditions. The movement amplitude of the artificial seabed presents a slight change during the initial stage of the drift-off (approximately 100 s ago) of the MODU and then increases rapidly. This is primarily attributed to the function that the telescopic joint could compensate for the offset of the MODU at the initial moment, in which condition the MODU would not exert excessive tension on the artificial seabed through the drilling riser. However, as the MODU drifts, the telescopic joint gradually reaches the limiting stroke, leading to an increasing movement amplitude of the artificial seabed. Hence, the MODU would impose excessive tension on the artificial seabed through the drilling riser. The displacement of the artificial seabed along the x-axis is the most significant due to the MODU mainly drifting along the x-axis and imposing the drift-off force on the artificial seabed by the drilling riser. There is an offset displacement with the y-axis, which is due to the forces imposed by the MODU on the artificial seabed through the drilling riser will separate along the y-axis since the inner buoys supporting the BOP and riser system is not at the center of the artificial seabed, which also results in the large amplitude of rotation of the artificial seabed around the z-axis. The movement of the artificial seabed presents a relatively minor amplitude in the other three DOFs. The artificial seabed is subject to a minor risk of capsizing in that it does not generate significant rotational motions in the y and xaxis during drift-off process. Nevertheless, the translational displacement of the artificial seabed along the x and y-axis, and the rotation angle along the z-axis are obvious, which can impose excessive tension and torsional forces on the tendon system of the artificial seabed. In practical operations, the tension and torsional forces of the tendon system should be monitored with focusing on the drift-off process of the MODU to prevent the collapse of the artificial seabed due to failure of the tendon system.

4.3. Dynamic drift-off response characteristics investigations of critical parameters in determining the physical limit

The fully coupled dynamic drift-off analysis of the MODU-DAS drilling system is carried out to investigate the dynamic response characteristics of critical parameters in determining the physical limit. The value of each parameter is expressed in a normalized way. The purpose

Table 5Structure parameters of DAS drilling system.

Artificial seabed	Value	Tendon	Value	Drilling riser	Value	Tieback casing	Value
Hight of outer artificial seabed (m)	16	Nominal wet weight of tether (kg/m)	83.1	Outer diameter (m)	0.5334	Outer diameter (m)	0.3397
Outer diameter of outer artificial seabed (m)	32	Diameter of tether (m)	0.163	Wall thickness (m)	0.0254	Wall thickness (m)	0.01425
Hight of skirt (m)	4	Minimum breaking load of tether (N)	2.15e ⁷	Length of single drilling riser (m)	22.86	Length of single tieback casing (m)	22.86
Outer diameter of skirt (m)	40	Axial stiffness of tether (N)	1.817e ⁶	Wet weight of single drilling riser (te)	2.038	Wet weight of single tieback casing (te)	0.491
Hight of inner artificial seabed (m)	20	Length of upper chain (m)	70	Steel grade	X-80	Steel grade	X-80
Outer diameter of inner artificial seabed (m)	7.8	Length of lower chain (m)	50	Material density (kg/m ³)	7850	Material density (kg/m ³)	7850
Capacity (te)	9009	Nominal wet weight of chain (kg/m)	454	Rotational stiffness of flex joint (kN·m/deg)	150	Length of upper stress joint (m)	5
Installation depth (m)	200	Minimum breaking load of chain (N)	2.27e ⁷			Length of lower stress joint (m)	10

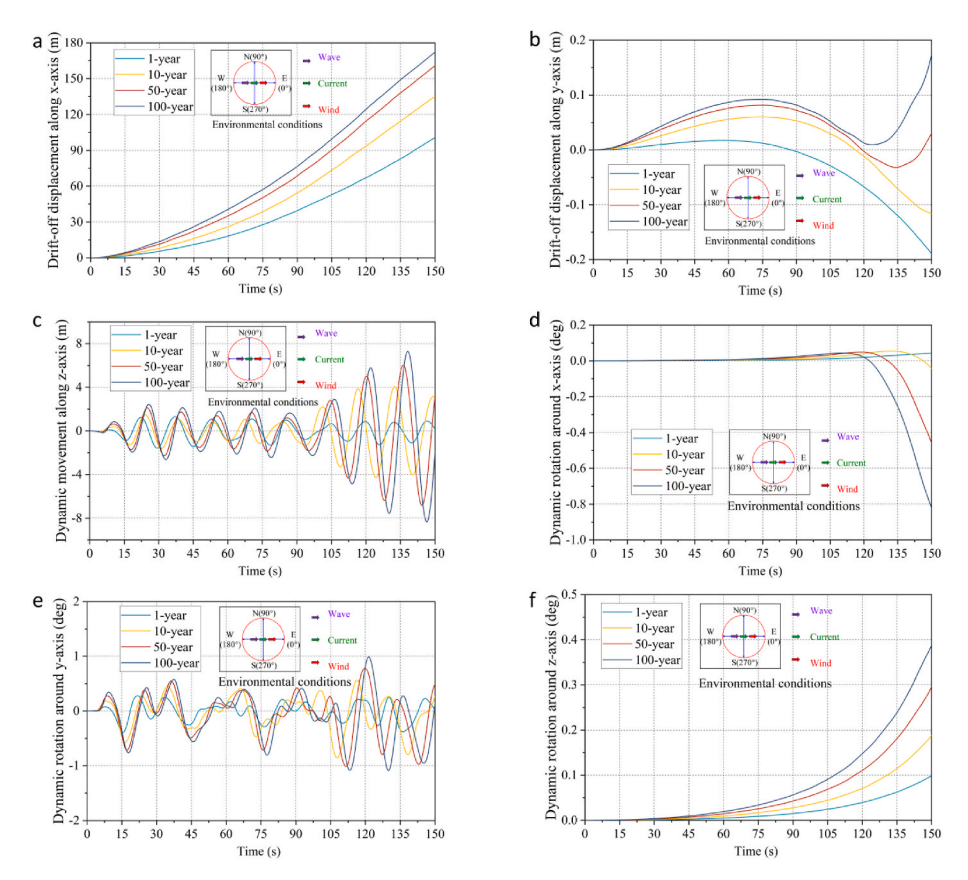


Fig. 6. The drift-off trajectory of the MODU.

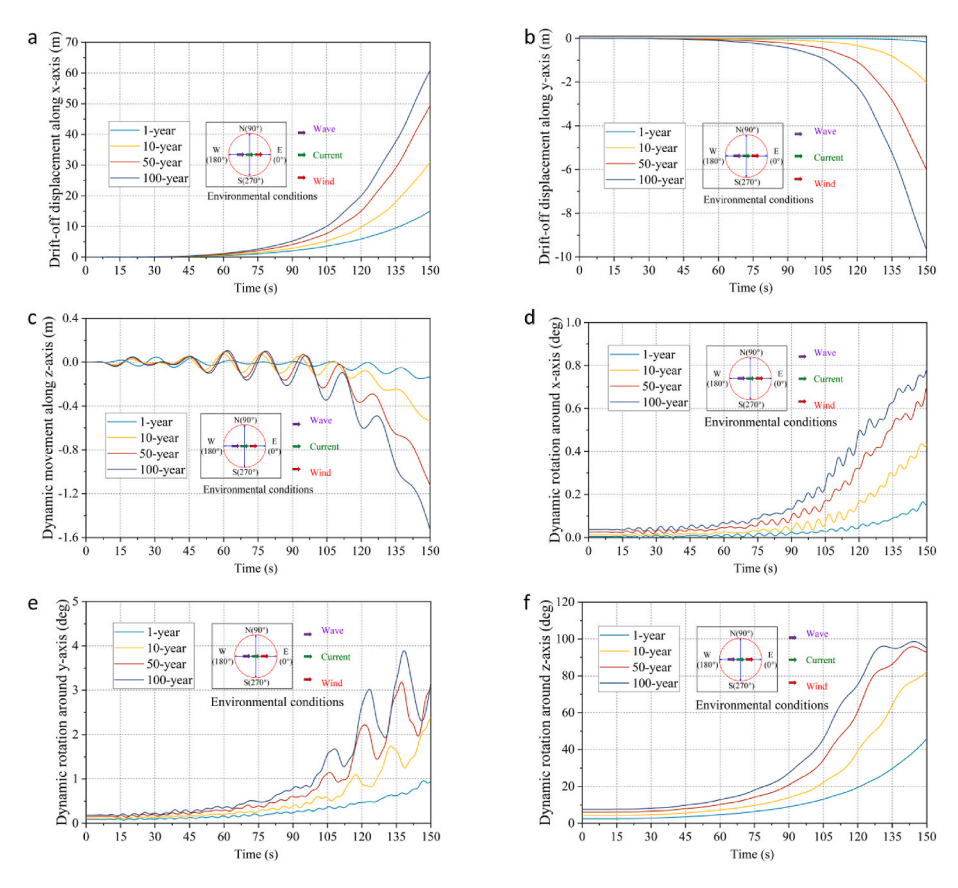


Fig. 7. Movement characteristics of the artificial seabed during drift-off process of the MODU.

is to identify the parameters that firstly reach the failure value from all critical parameters to determine the physical limit.

Fig. 8 presents the dynamic response results of the critical parameters under different return periods of environmental conditions when the incident direction is along the MODU's bow. It should be noted that none of the critical parameter values are zero at the initial moment because statics calculation is firstly performed in the FEM program to provide a starting configuration for a dynamic simulation. All dynamic response curves of the critical parameters exhibit a wave-shaped pattern due to the 6-DOF motions resulting from the transient response of the MODU to waves. The parameter response speed of the drilling riser system is significantly faster than that of the tieback casing system, and the critical parameters of the tieback casing system are almost unchanged during the initial stage of the drift-off of the MODU, which is mainly due to the inertia effect of the whole system and the inhibiting effect of the artificial seabed. The effect of the movements of the MODU is transmitted from top to bottom along the drilling riser. The artificial seabed can reduce this effect, leading to a significantly lower parameters response speed of the tieback casing than the drilling riser. The parameter which firstly reaches the failure value under all environmental conditions is the declination of the lower flex joint. The increase of the return period of environmental conditions would accelerate the dynamic response speed of potential offset limiting parameters and shortens the time for the declination of the lower flex joint to reach the failure value. As the environmental condition's return period increases from 1-year to 100-year, the time for the lower flex joint's declination to reach the failure value decreases from 116 s to 77.2 s with decreasing rate of 33.4%. The reason is that the increase of environmental conditions promotes the drift-off velocity of the MODU per-unit time. Conversely, it increases the gradient variation of the lower flex joint's declination and reduces the time taken to reach the failure value.

4.4. Dynamic drift-off warning limits of MODU

Fig. 9 presents the principle for establishing the drift-off warning limits of MODU when the incident direction of environmental conditions is along with the bow of the MODU. The time for the MODU drifts to reach the physical limit is 116 s as shown in Fig. 9. The drift-off displacement from the original location is 63.1 m, at which the EDS

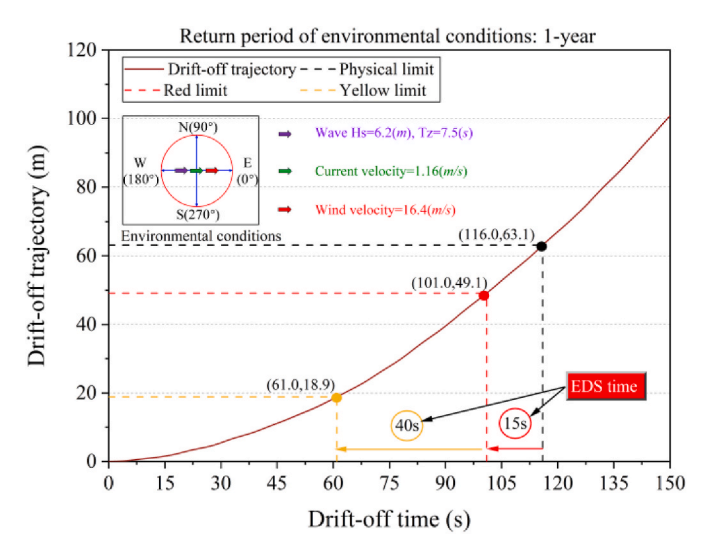


Fig. 9. Principle of drift-off warning limits determination.

must be completed. It takes 15 s from the activation to the completion of the EDS. Hence, the EDS must be activated within 101 s and drift-off displacement of the MODU at this moment is 49.1 m. Simultaneously the red limit should be established. 40s are needed from preparation to activation of EDS. Consequently, the EDS must be prepared within 61 s, with a drift-off displacement of 18.9 m for the MODU, which represents the yellow limit.

Fig. 9 provides the drift-off warning limits of MODU for a single environmental condition's incident direction. In practical operations, the direction of the environmental conditions varies randomly from 0° to 360° . Consequently, this paper further investigates the drift-off motion characteristics of the MODU when the incident direction of environmental conditions is from 0° to 360° . And the complete drift-off warning limits for each environmental condition's return period from 0° to 360° are established and plotted in a polar coordinate diagram, as illustrated in Fig. 10.

As can be seen from Fig. 10, the drift-off warning limits of the MODU

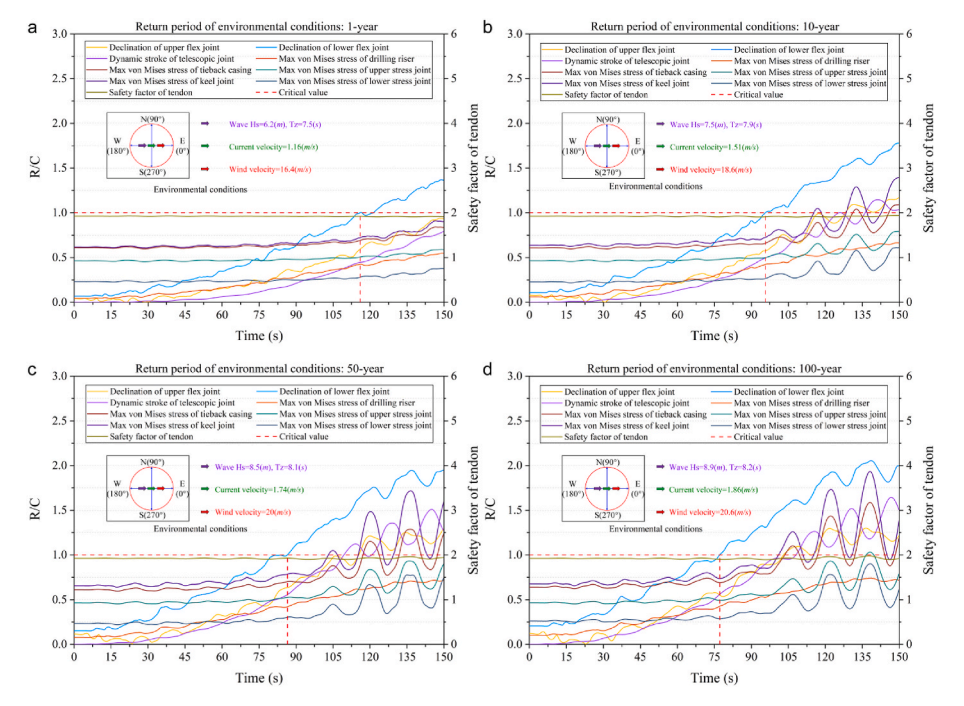


Fig. 8. Dynamic response of critical parameters in determining the physical limit.

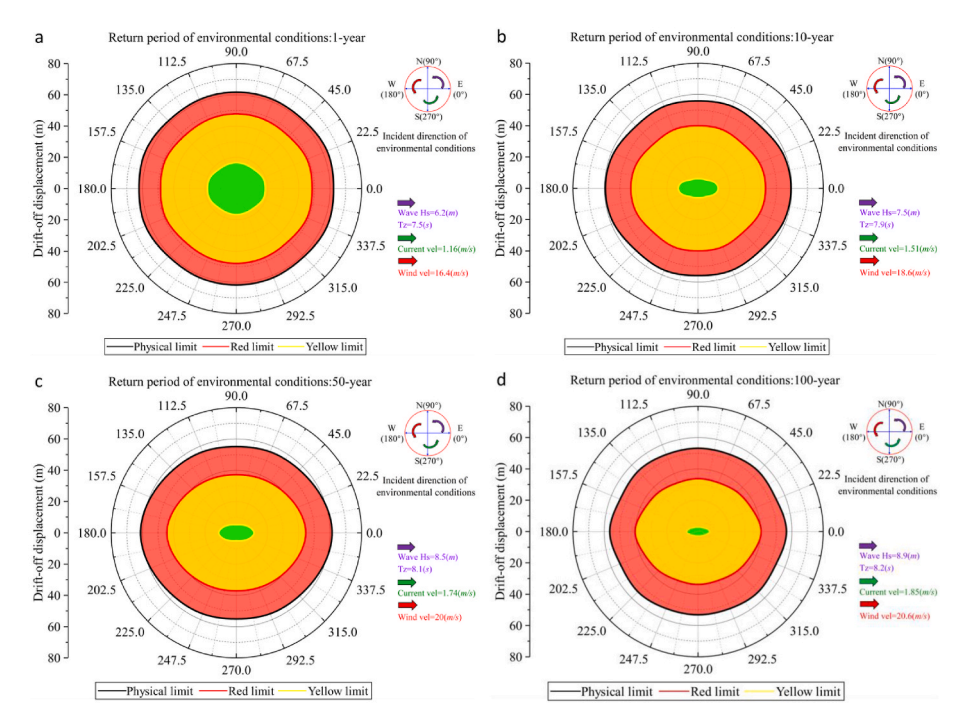


Fig. 10. Dynamic drift-off warning limits of MODU with DAS drilling system.

are almost symmetrical in horizontal and vertical directions in that the DAS drilling system is almost geometrically symmetrical. The slight difference is that IBCs are not located in the central position of the artificial seabed. It can be reflected that the magnitude of the environmental conditions has a significant effect on the drift-off warning limits. An increase in environmental conditions will cause a reduction of the drift-off warning limits. It should be noted that there are different mechanisms that cause the physical limit, the red limit and the yellow limit to become smaller with increasing of environmental conditions. The cause of the physical limit becoming slightly smaller with increasing environmental conditions result from the splitting force from the drilling riser along the horizontal direction and the current force together promote the rotation of the lower flex join. As the current force increases, the declination of the lower flex joint reaches its failure criterion more easily leading to a smaller physical limit of the MODU. However, the red and the yellow limits decrease with increasing environmental conditions is that increasing environmental conditions promote a longer drift-off distance of the MODU for the same EDS's operating time. As a result, the red and yellow limits are located further away from the physical limit. It should be noted that the red and yellow limits are determined through the backward deduction of MODU's trajectory.

In addition, the incident direction of environmental conditions has minor effect on the physical and red limits, but contributes to an obvious influence on yellow limit. When the incident direction of environmental conditions varies from 0° to 360°, the shape of physical limit approximately presents a circle, while the shape of red and yellow limits is approximately elliptical. In all cases studied in this paper, the first critical offset limiting parameter to reach the failure value is the declination of the lower flex joint. Regardless of the change in the incident direction of the environmental loads, the drift-off distances of the MODU are almost constant at the time when the declination of the lower flex joint reaches its failure value, so the shape of the physical limit approximately presents a circle. The reason that the red and yellow limits are approximately elliptical is that when the environmental conditions are incident from 0° to 90° , the total load on the MODU increases due to the increased force area, resulting in the platform drifting farther away within the same EDS operation time, which causes the red limit to be established farther from the physical limit, and similarly, the yellow

limit is established farther from the red limit. The ratio of the short axis to the long axis of the yellow limit ellipse is smaller than the red limit, because the operating time of EDS is longer from the yellow limit to the red limit than from the red limit to the physical limit.

The numerical results of the drift-off warning limits for the MODU with new DAS drilling system demonstrate that the MODU has sufficient drift-off range, allowing operators ample time to safely disconnect the drilling riser system from the BOP in moderate sea conditions. Even in the event of extreme sea conditions, it can also ensure the safe disconnection of the drilling riser system without damaging the drilling equipment as long as the operators can timely detect the fault of the DP system. However, it should be noted that the EDS should be prepared to activate as early as possible when the environmental conditions increase. In addition, the operator's preparation time for EDS becomes more demanding when the incident direction of the environmental conditions changes from parallel to perpendicular to the MODU's bow under the same environmental conditions.

4.5. OED-BPNN-GA based parameter sensitivity analysis

Fig. 14 presents the parameters sensitivity results of drift-off warning limits obtained by employing the OED-BPNN-AG method. In this work, a three-layer BPNN is constructed, comprising an input layer, a hidden layer and an output layer. The input layer contains 9 neurons representing nine parameters in Table 3, the hidden layer contains 10 neurons, and the output layer contains a neuron representing the yellow limit, red limit or physical limit. In the input and output layers, each neuron contains 32 samples obtained from ODE and numerical simulations. The 32 samples are split into a training set and a test set for training and testing the BPNN respectively, where the training set comprises 22 samples and the test set comprises 10 samples, that is, the ratio of the training set to test set is 7:3. During the training process, the maximum number of iterations is 1000 and the Bayesian regularization optimization algorithm is used. The performance of the well-trained BPNN is evaluated by the R² obtained from the regression analysis, in which R represents the correlation coefficient between the target and the predicted values. The regression analysis results of the yellow limit, red limit and physical limit are presented in Fig. 11, Fig. 12, and Fig. 13,

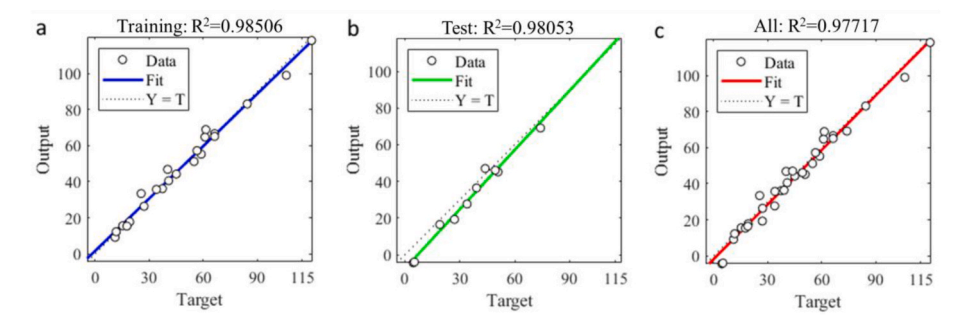


Fig. 11. The correlation coefficient between target and predicted values for yellow limit.

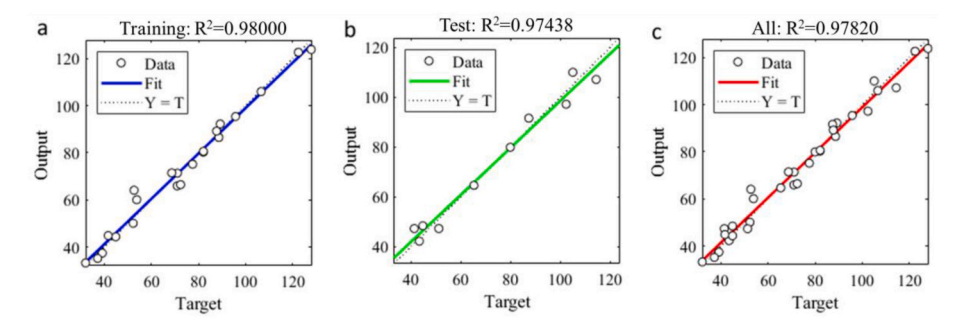


Fig. 12. The correlation coefficient between target and predicted values for red limit.

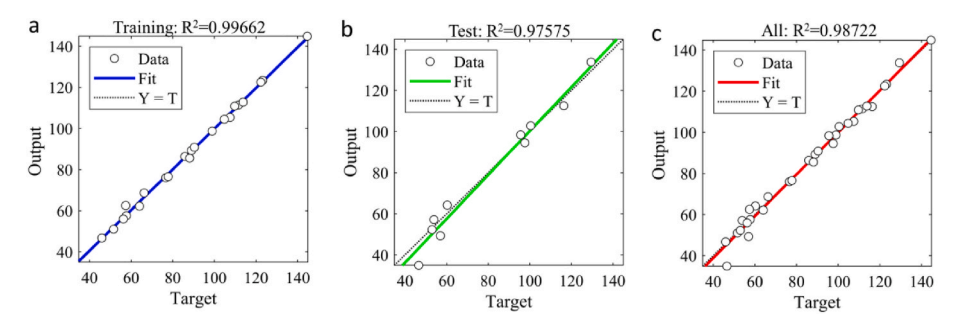


Fig. 13. The correlation coefficient between target and predicted values for physical limit.

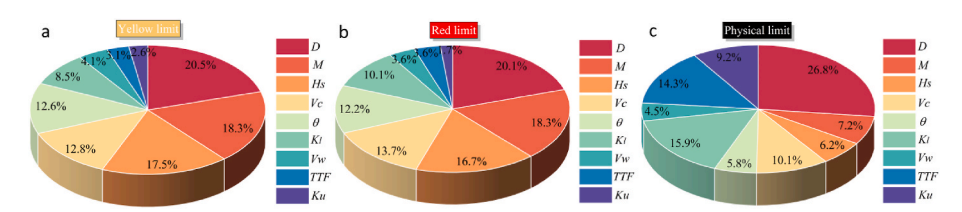


Fig. 14. The relative importance of the critical impact parameters for drift-off warning limits.

respectively. The horizontal and vertical coordinates represent the results of the numerical simulations and the BPNN predictions, respectively. Generally, the accuracy of the model is assumed to be sufficient when the R^2 is more than 0.9 (Zhu et al., 2020). As can be seen from Figs. 11–13, the R^2 are all higher than 0.97, proving the high accuracy of the BPNN.

As can be observed from Fig. 14 that each parameter contributes in varying magnitudes to the yellow, red and physical limits, in which the installation depth of the artificial seabed (*D*) contributes the most to all three warning limits, with values of 20.5%, 20.1% and 26.8%, respectively. This is because as the installation depth of the artificial seabed increases, the distance between the location of the drift-off warning

limits and the original position of the MODU increases significantly as the lower flex joint's declination reaches its failure value. The magnitude of the contribution of each parameter is ranked identically in the yellow and red limits, but differs from the physical limit. This is primarily because that the method of establishing the physical limit is different from the yellow and red limits. For the yellow and red limits, the installation depth of the artificial seabed is the most important influencing parameter, followed by the quality of the MODU (M), the significant wave height ($H_{\rm s}$) and the current velocity ($V_{\rm c}$), as these parameters contribute to the change in the drift-off distance of the MODU by influencing the drift-off velocity within the time given by EDS. For the physical limit, the installation depth of the artificial seabed is the

most important influencing parameter, followed by the rotational stiffness of the lower flex joint (K_1) and the top tensioned factor (TTF). The increase in both the K_1 and the TTF allows the physical limit to be located further from the original position of the MODU, which is due to that the large value of the K_1 and the TTF have a more powerful ability to inhibit the declination of the lower flex joint. The above parameters that have a major impact on the physical limit are design parameters. In addition, the $V_{\rm C}$ belonging to the environmental parameter poses a significant impact on physical limit. The higher the current velocity, the closer the position of the physical limit is to the original position of the MODU. This is because that the high current velocity exerts dragging forces on the drilling riser, resulting in the increased lateral deformation of the drilling riser. Consequently, the declination of the lower flex joint becomes larger and it is easier to reach the failure value. Other limiting parameters have a slight contribution of less than 10%.

5. Conclusions

This study focuses on the dynamic drift-off warning limits for dynamically positioned MODU with the DAS drilling coupling system to promote the safety of DP drilling operations. A three-phase method for establishing the dynamic drift-off warning limits is developed, and the drift-off warning limits of the MODU are determined by analyzing the fully coupled drift-off process of the MODU-DAS drilling system. A quantitative method for parameter sensitivity analysis based on ODE-BPNN-GA is proposed, and the sensitivity analysis of critical parameters on the drift-off warning limits is investigated. The following conclusions can be obtained:

- (1) Harsh environmental conditions would aggravate the movement amplitude of the MODU and artificial seabed. Moreover, the dynamic response speed of each critical parameter would be accelerated. The artificial seabed motions will cause excessive tension and torsional forces on its tendon system. In practical engineering applications, the tension and torsional forces of the tendon system should be monitored with focusing on the drift-off process of the MODU.
- (2) In all cases study in this paper, the declination of the lower flex joint is the parameter that firstly reach the failure value during the drift-off process of the MODU. Consequently, the focus is to monitor the dynamic changes of the lower flex joint's declination during the drift-off process of MODU.
- (3) Both the magnitude and incident direction of the wave, wind, and current affect the drift-off warning limits. Severer environmental conditions will reduce the area of the drift-off warning limits. It is recommended that operators should activate EDS as early as possible when the environmental conditions increase or its direction changes from parallel to perpendicular to the MODU's bow.
- (4) Each parameter contributes various magnitudes to the yellow, red, and physical limits. The installation depth of the artificial seabed is the largest contributing parameter. Therefore, the driftoff warning limits can be enlarged by appropriately increasing the installation depth of the artificial seabed according to the service sea conditions of the DAS drilling system.

Based on the DAS drilling system, the paper initially investigates a methodology for establishing dynamic drift-off warning limits of MODU as well as verifies its practicability. Nevertheless, the DP's control equations are not considered in the model established in this paper, and the selected operating cases are subject to limitations. In the future, it is proposed to integrate the DP's control equations into the FEM solver by taking into account the factors including the failure number and location of the thrusters to develop a more accurate coupled dynamic model. In addition, integrating neural network algorithms with dynamic drift-off warning limit methods to establish real-time response dynamic drift

warning limits is a forward-looking and innovative research.

CRediT authorship contribution statement

Xingwei Zhen: Conceptualization, Methodology, Formal analysis, Writing – original draft, Funding acquisition. **Wei Guo:** Methodology, Formal analysis, Writing – original draft. **Zhengru Ren:** Writing – review & editing, **Yi Huang:** Writing – review & editing, Supervision.

Declaration of competing interest

The authors declare that they have no known competing financial interests or personal relationships that could have appeared to influence the work reported in this paper.

Data availability

Data will be made available on request.

Acknowledgements

The research is financially supported by the National Natural Science Foundation of China (No. 52171249), the Natural Science Foundation of Liaoning Province (No.2023-MS-117) and the Fundamental Research Funds for the Central Universities (DUT22LK26).

Nomenclature

BPNN Back Propagation Neural Network

DAS Deepwater Artificial Seabed

DOF Degree-of-Freedom
DP Dynamic Positioning

EDS Emergency Disconnect Sequence

FEM Finite Element Model FSDR Freestanding Drilling Riser FPU Floating Production Unit

GA Garson's Algorithm
IBC Inner Buoyancy Can

MODU Mobile Offshore Drilling Unit

M.W.L Mean Water Level

OED Orthogonal Experimental Design
QTF Quadratic Transfer Function
RAO Response Amplitude Operator
STLP Subsurface Tension Leg Platform

TTF Top Tensioned Factor

References

API, 1998. Design of Risers for Floating Production Systems (FPSs) and Tension-Leg Platforms (TLPs). API RP 2RD.

API, 2015. Design and Analysis of Stationkeeping Systems for Floating Structures. API, RP 2SK.

Bhalla, K., Cao, Y.C., 2005. Watch circle assessment of drilling risers during a drift-off and drive-off event of a dynamically positioned vessel. In: MTS DynamicPositioning Conference (Houston, Texas).

Chang, Y.J., Chen, G.M., Wu, X.F., Ye, J.H., Chen, B., Xu, L.B., 2018. Failure probability analysis for emergency disconnect of deepwater drilling riser using Bayesian network. J. Loss Prev. Process. Ind. 51, 42–53.

Chen, H.B., Moan, T., Harry, V., 2008. Safety of dynamic positioning operations on mobile offshore drilling units. Reliab. Eng. Syst. Saf. 93 (7), 1072–1090.

Cheng, X., Li, G.Y., Robert, S., Pierre, M., Chen, S.Y., Hildre, H.P., Zhang, H.X., 2019. Data-driven uncertainty and sensitivity analysis for ship motion modeling in offshore operations. Ocean Eng. 179, 261–272 (S).

Childers, M., 2005. Surface BOP, Slim Rise or Conventional 21-inch Riser - what Is the Best Concept to Use. Society of Petroleum Engineers (SPE), Amsterdam, Netherlands. de Pina, A.C., de Pina, A.A., Albrecht, C.C., Leite Pires De Lima. B.S., Jacob. B.P., 2013.

de Pina, A.C., de Pina, A.A., Albrecht, C.C., Leite Pires De Lima, B.S., Jacob, B.P., 201 ANN-based surrogate models for the analysis of mooring lines and risers. Appl. Ocean Res. 41, 76–86.

Dotta, R., Tannuri, E.A., De Mello, P.C., Diederichs, G.R., Cruz, D.F., Oshiro, A.T., 2018. Validation of Numerical Models for the Drift-Off Study in Drilling Vessels Using Full

- Scale Measurements. American Society of Mechanical Engineers (ASME), Madrid, Spain.
- Duan, Q.Y., Zhen, X.W., Huang, Y., Yao, J.J., Guo, W., Liu, G., 2022. Experiment-based coupled dynamic analysis of submerged production platform-mooring system in internal solitary waves. Ocean Eng. 260, 112044.
- Garson, G.D., 1991. Interpreting neural network connection weights. AI Expet. 6, 47–51.
 Gjerde, T., Chen, H.B., 2014. Probabilistic RED Limit Study for Mobile Offshore Drilling Units. American Society of Mechanical Engineers (ASME), San Francisco, CA, United states
- Guo, Y.F., Ji, S.J., Ye, A.J., 2006. New Device for Drilling in Deepwater under Semisubmersible: ABS Unit. Society of Petroleum Engineers, Bangkok, Thailand.
- Han, Y., Zhen, X.W., Huang, Y., 2021a. Drift-off warning limits for dynamically positioned FPSO and Deepwater Artificial Seabed (DAS) coupling system. Ocean Eng. 237, 109662.
- Han, Y., Zhen, X.W., Moan, T., Huang, Y., 2021b. Real time prediction of operational safety limits for dynamic positioning of an FPSO in a Deepwater Artificial Seabed system. Mar. Struct. 80, 103093.
- IMCA, 2006. Analysis of Station Keeping Incident Data 1994-2003. IMCA, p. 181. IMCA, 2016. Dynamic Positioning Station Keeping Incidents, 2001-2012. IMAC, p. 231.
- Kim, J.H., Kim, Y., Lu, W.J., 2020. Prediction of ice resistance for ice-going ships in level ice using artificial neural network technique. Ocean Eng. 217, 108031.
- Laik, S., 2018. Offshore Petroleum Drilling and Production. CRC Press.
- Lim, F., Lim, T.K., Guo, Y.F., Ji, S.J., Xu, L.B., 2008. Near-surface BOP drilling system. In: The Eighteenth International Offshore and Polar Engineering Conference.
- Liu, X.Q., Chen, G.M., Chang, Y.J., Ji, J.Q., Fu, J.J., Song, Q., 2016. Drift-off warning limits for deepwater drilling platform/riser coupling system. Shiyou Kantan Yu Kaifa/Petroleum Exploration and Development 43 (4), 641–646 and 668.
- Liu, X.Q., Chen, G.M., Ji, J.Q., Fu, J.J., 2017. Coupled dynamic analysis on the drive-off of deepwater platform/riser system. Mechanika 23 (2), 259–264.
- Liu, X.Q., Zhang, S.Y., Chen, G.M., Chang, Y.Y.J., Xu, L.B., Sheng, L.X., 2019. Fully Coupled Drift-Off Analysis of Platform/riser/inner Pipe System for Deepwater Drilling. International Society of Offshore and Polar Engineers, Honolulu, HI, United crates.
- Morison, J.R., Johnson, J.W., Schaaf, S.A., 1950. The force exerted by surface waves on Piles. J. Petrol. Technol. 2 (5), 149–154.
- Nguyen, C., Thethi, R., et al., 2006. Storm-safe Deepwater Drilling, Bangkok, Thailand. Society of Petroleum Engineers (SPE).
- Nie, Z.Y., Chang, Y.J., Liu, X.Q., Chen, G.M., 2019. A DBN-GO approach for success probability prediction of drilling riser emergency disconnect in deepwater. Ocean Eng. 180, 49–59.
- OCIMF, 1994. Prediction of Wind and Current Loads on VLCCs. Witherby & Co., London. Orcina, 2018. OrcaFlex, Version 10.3a.
- O'Sullivan, E., Soles, J., Dib, M., 2004. Fully Coupled EDS/drift-off Analysis for a Harsh Environment, Deepwater Site. American Society of Mechanical Engineers, Vancouver, BC, Canada.
- Poirier, M., Russo, M., Srikonda, R., Karlstad, M., Abelsen, K., Kling, C., 2018. The development of an enhanced riser management system including dynamic watch circles for drilling operations in Harsh and ultra-deepwater environments. In: ASME 2018 37th International Conference on Ocean, Offshore and Arctic Engineering.
- Quéau, L.M., Kimiaei, M., Randolph, M.F., 2015. Sensitivity studies of SCR fatigue damage in the touchdown zone using an efficient simplified framework for stress range evaluation. Ocean Eng. 96, 295–311.
- Quigley, C., Williams, D., 2015. A Revised Methodology for the Calculation of Modu Watch Circles. American Society of Mechanical Engineers (ASME), St. John's, NL, Canada
- Ren, Z.R., Han, X., Yu, X.J., Skjetne, R., Leira, B.J., Svein, S., Zhu, M., 2023. Data-driven simultaneous identification of the 6DOF dynamic model and wave load for a ship in waves. Mech. Syst. Signal Process. 184, 109422.

- Shen, H.Y., Wang, Z.X., Gao, C.Y., Qin, J., Yao, F.B., Xu, W., 2008. Determining the number of BP neural network hidden layer units. J. Tianjin Univ. Technol. 24 (5), 13–15.
- Tannuri, E.A., de Mello, P.C., Dotta, R., Oshiro, A.T., Diederichs, G.R., Cruz, D.F., Ferreira, M.D., Nunes, L.M.P., Maeda, K., 2020. Drift-off study in drilling vessels comparing numerical model and full-scale field measurements. J. Offshore Mech. Arctic Eng. 142 (4).
- Teixeira, F.J.R., Oshiro, A.T., Tannuri, E.A., 2014. Drifting Time of a Standard Drillship.

 American Society of Mechanical Engineers (ASME), San Francisco, CA, United states.
- Wang, C., Li, G., Skulstad, R., Cheng, X., Osen, O., Zhang, H., 2021. A sensitivity quantification approach to significance analysis of thrusters in dynamic positioning operations. Ocean Eng. 223, 108659.
- Wang, L., Zeng, Y., Chen, T., 2015. Back propagation neural network with adaptive differential evolution algorithm for time series forecasting. Expert Syst. Appl. 42 (2), 855–863
- Wang, S., Donnarumma, S., 2012. Drift-off and Drive-Off Assessment of a Dynamically Positioned Drillship. Texas Section of the Society of Naval Architects and Marine Engineers, Houston, TX, United states.
- Wu, H., 2013. Application of Orthogonal Experimental Design for the Automatic Software Testing. Applied Mechanics and Materials. Trans Tech Publ.
- Wu, J.H., Zhen, X.W., Liu, G., Huang, Y., 2019. Optimization design on the riser system of next generation subsea production system with the assistance of DOE and surrogate model techniques. Appl. Ocean Res. 85, 34–44.
- Wu, J.H., Zhen, X.W., Liu, G., Huang, Y., 2021. Uncertain multidisciplinary design optimization on next generation subsea production system by using surrogate model and interval method. China Ocean Eng. 35 (4), 609–621.
- Xie, C., Zhou, L., Ding, S.F., Liu, R.W., Zheng, S.J., 2023. Experimental and numerical investigation on self-propulsion performance of polar merchant ship in brash ice channel. Ocean Eng. 269, 113424.
- Zhu, X.M., Sun, L.P., Li, B., 2020. Dynamic analysis of vessel/riser/equipment system for deep-sea mining with RBF neural network approximations. Mar. Georesour. Geotechnol. 38 (2), 174–192.
- Zhen, X.W., Huang, Y., Zhang, Q., 2014. Parametric study on the effects of flexible jumpers on the global behavior of the rigid riser based on an innovative subsurface tension leg platform. J. Ship Mech. 18 (6), 711–723.
- Zhen, X.W., Huang, Y., 2017. Parametric study on the behavior of an innovative subsurface tension leg platform in ultra-deep water. China Ocean Eng. 31 (5), 590, 507
- Zhen, X.W., Huang, Y., Zhang, Q., 2018a. Investigations on the mechanical behavior of an innovative subsurface tension leg platform in ultra-deep water (Part I). J. Ship Mech. 22 (3), 311–324.
- Zhen, X.W., Wu, J.H., Huang, Y., Han, Y., Yao, J.J., 2018b. Parametric dimensional analysis on the structural response of an innovative subsurface tension leg platform in ultra-deep water. China Ocean Eng. 32, 482–489.
- Zhen, X.W., Moan, T., Gao, Z., Huang, Y., 2018c. Risk assessment and reduction for an innovative subsurface well completion system. Energies 11 (5), 1306.
- Zhen, X.W., Vinnem, J.E., Han, Y., Peng, C.Y., Yang, X., Huang, Y., 2020. New risk control mechanism for innovative deepwater artificial seabed system through online risk monitoring system. Appl. Ocean Res. 95, 1–9
- risk monitoring system. Appl. Ocean Res. 95, 1–9.

 Zhen, X.W., Guo, W., Duan, Q.Y., Du, W.J., Huang, Y., 2022a. Transient response of an innovative Deepwater Artificial Seabed (DAS) system under tendon failure conditions. Ocean Eng. 266, 113063.
- Zhen, X.W., Duan, Q.Y., Han, Y., Huang, Y., 2022b. Investigations on the quasi-static stability behavior of an innovative subsurface tension leg platform in ultra-deep water (part II). J. Ship Mech. 26 (6), 834–842.
- Zhen, X.W., Ning, Y.N., Du, W.J., Huang, Y., Vinnem, J.E., 2023. An interpretable and augmented machine-learning approach for causation analysis of major accident risk indicators in the offshore petroleum industry. Process Saf. Environ. Protect. 173, 922–933.